Effect of the Rashba splitting on the RKKY interaction in topological-insulator thin films

Mahroo Shiranzaei,[1] Hosein Cheraghchi,[1,*] and Fariborz Parhizgar[2,†]
[1]*School of Physics, Damghan University, P.O. Box 36716-41167, Damghan, Iran*
[2]*School of Physics, Institute for Research in Fundamental Sciences (IPM), Tehran 19395-5531, Iran*
(Received 6 February 2017; revised manuscript received 20 May 2017; published 12 July 2017)

We investigate the effect of Rashba splitting on the Ruderman-Kittel-Kasuya-Yosida (RKKY) interaction in a topological-insulator (TI) thin film both at finite and zero chemical potential. We show that the spin susceptibility of the TI thin film depends strongly on the direction of the distance vector between impurities. In addition to the well-known Heisenberg-, Ising-, and Dzyaloshinskii-Moria (DM)-like terms reported before in TIs, we find another term in the off-diagonal part of the spin-susceptibility tensor which is symmetric in contrast to the DM term. Furthermore, we show how one can tune the RKKY interaction by using electric field applied perpendicularly to the surface plane of the TI, where in the presence of such a field the RKKY interaction can be enhanced drastically for small chemical doping. We present our results for two different situations, namely intersurface pairing of magnetic impurities as well as intrasurface pairing. The behavior of these two situations is completely different, which we describe by mapping the density of states of each surface on the band dispersion.

DOI: 10.1103/PhysRevB.96.024413

I. INTRODUCTION

Among magnetic interactions that have been detected in materials, Ruderman-Kittle-Kasuya-Yosida (RKKY) [1–3], an indirect exchange interaction between two magnetic adatoms via host itinerant electrons, is one of the main reasons for coupling between magnetic impurities. This interaction is proportional to the spin susceptibility of the host material and so gives the spin information of the system [4,5]. Depending on the spin structure of the material, different types of couplings between magnetic adatoms can occur via the RKKY interaction. While in spin-degenerate systems, such as graphene [6–9], two localized magnetic impurities are coupled to each other in the form of an isotropic collinear Heisenberg-like term, the anisotropic collinear Ising-like term with different coefficients in different spin directions appears in spin-polarized systems [5,10,11]. Moreover, in materials with Rashba spin-orbit coupling [12–14] as well as materials with spin-valley coupling [4,15,16], it has been shown that twisting the RKKY interaction is possible by the antisymmetric noncollinear Dzyaloshinskii-Moria (DM)-like term [17,18]. The RKKY interaction is a long-range interaction that usually decays as R^{-D}, with D the dimension of the system, which oscillates with respect to the distance between impurities and the electron's Fermi wave vector. However, depending on the band structure of the system, such behavior may change. This fascinating feature of this mechanism is measurable in experimental observations by angle-resolved photoemission spectroscopy (ARPES) and scanning tunneling microscopy (STM) in the study of magnetotransport and single-atomic magnetometry [15,19–21].

The RKKY interaction can be in charge of diverse magnetic phases and ordering in metals and semiconductors [6,22,23] such as ferromagnetic and antiferromagnetic ordering [24–28] as well as spin glass [29,30] and spiral phases [15,31]. Recently, the quantum anomalous Hall effect (QAHE) has been predicted theoretically [32] and realized experimentally [33–35] in magnetically doped three-dimensional (3D) topological insulators (TIs). Since such experiments need the ferromagnetic coupling between magnetic adatoms, it brings intensive attention to the mechanism of the coupling among magnetic impurities in this class of materials. Although the RKKY interaction (and, more precisely, its zero chemical potential version, i.e., van Vleck mechanism) is thought to be the main mechanism of this coupling [36], such hypothesis is still under debate [37].

3D TIs, i.e., systems with gapped bulk states and gapless surface states protected by time-reversal symmetry (TRS), are a novel kind of material and have been the subject of much research during the past few years [38–40]. An important branch of topological insulators is bismuth-based structures, for instance, Bi_2Se_3 and Bi_2Te_3, which are made of van der Waals interacting layers known as quintuple layers (QLs) [41]. These structures behave as a topological insulator with gapless surface states for thicknesses above 6 QLs [42], where the surface's state has isotropic Dirac-type band dispersion, presented by an effective chiral Rashba-type Hamiltonian. The combination of the pure Rashba Hamiltonian with being in the category of Dirac materials [43] makes TIs a promising candidate for spintronic and electronic applications [44]. Since the bulk band gap of these 3D systems is not large enough, in practice, the bulk states usually play a severe role in experiments and so it is favorable to use the thin version of these structures in order to reduce the effect of bulk. It has been experimentally shown that for 5 QLs thickness and less, the states of different surfaces of the TI thin film would be hybridized. Although these ultrathin films are not 3D topological insulators with gapless surface states, they can share other interesting features such as a phase transition from quantum spin Hall insulator to a normal insulator [36,45–47], time-reversal topological superconductivity [48], and band tunability by applying perpendicular electric [36,48,49] or in-plane magnetic field [50]. Furthermore, magnetic topological insulators and their thin version [51,52] become important since the ordered magnetic impurities on the surface of the TI can create a pure magnetic field [53] and open a gap in

*cheraghchi@du.ac.ir
†fariborz.parhizgar@ipm.ir

the band dispersion, which has been observed experimentally [52]. Such intrinsic ferromagnetism can result in QAHE when the Fermi energy lies within the gap of the system.

The RKKY interaction in Rashba materials such as TIs has been explored extensively [12–14,54–57]. The existence of the strong Rashba spin-orbit coupling in these materials makes the RKKY interaction have a rich physics that includes a DM-like term [13] and can result in different magnetic phases such as ferromagnetic, paramagnetic, and spin glass [14]. In addition, such interaction on the surface of the TI has been investigated when a superconductor is present in the proximity of the TI [54]. Since the magnetic impurities perpendicularly ordered to the surface of the TI can produce a gap on the surface state, the RKKY interaction together with such gap has been investigated self-consistently [55,56]. While all of these theoretical investigations have been done for a thick 3D TI, the experimental realization of QAHE in the TI thin films makes it essential to investigate the RKKY interaction in the thin version of TIs where two surfaces are hybridized to each other [36].

In this work, we investigate the spin susceptibility of the TI thin film and derive the RKKY interaction both at zero and finite doping. In contrast to most of the previous works on TIs, we find strong spatial anisotropy of the RKKY interaction with respect to the direction of the connecting line between impurities when one or both impurities have an in-plane spin component projected on the surface of the TI [55,56]. We explore the effect of parameters such as chemical potential, tunneling strength between surfaces, and applied biased electric field on the RKKY interaction. The last one has the benefit that one can electrically tune the RKKY interaction and, as a result, the magnetic properties. We describe our findings by means of the contribution of the top and bottom surface states in the band dispersion. The organization of the paper is as follows: In Sec. II, we introduce the theory of the work starting from the model Hamiltonian. In this part, we present the contribution of the top and bottom surfaces in the band dispersion separately, which is useful in the description of our results. Next, we report our method for calculating the RKKY interaction by using the real-space Green's function. To guarantee fluency, we have presented the analytic results for the real-space Green's functions in Appendix A and details of the RKKY Hamiltonian have been given in Appendix B. Section III presents our results where we discuss the RKKY interaction between impurities on the same and different surfaces. We have summarized and concluded our results in Sec. IV.

II. THEORY

A. Model Hamiltonian

The surface states of the TI thin film around the Γ point can be described by the effective two-dimensional Hamiltonian [42,47,58]

$$H_0(\mathbf{k}) = -D\,k^2\tau_0\otimes\sigma_0 + \tau_z\otimes[\hbar v_F(\sigma\times\mathbf{k})\cdot\hat{z} + V\sigma_0] + \Delta\tau_x\otimes\sigma_0, \quad (1)$$

where σ, τ are Pauli matrices in spin and surface space, respectively, $\mathbf{k}=(k_x,k_y)$ represents the wave vector of the surface state's electrons, and v_F is their Fermi velocity. The term with coefficient D refers to the particle-hole asymmetry in the system and V shows the potential difference between surfaces which can be produced by the effect of substrate or an external electric field applied perpendicularly to the surfaces.

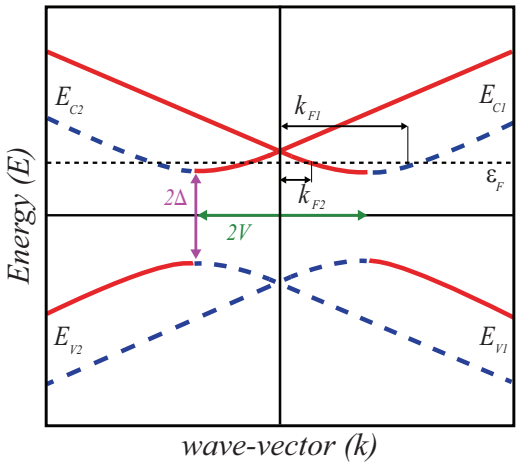

FIG. 1. Schematic figure shows the dispersion of TI thin film and illustrates two Fermi wave vectors, $k_{F1,2}$, and the Fermi energy ε_F by the dotted line.

The last term in Eq. (1) shows the tunneling between different surfaces and has the form $\Delta-\Delta_1 k^2$, where the Δ_1 term in special thin films in which $\Delta\,\Delta_1>0$ leads to a topological phase transition from a quantum spin Hall insulator to a normal insulator as V passes the critical value $\hbar v_F\sqrt{\Delta/\Delta_1}$ [36,47]. The effect of this term is important for finite-size nanoribbons of TI thin film where a topological transition induced by Δ_1 can lead to the emergence of zero-energy modes at the nanoribbon edges and, considering this term for the bulk, affects the results quantitatively but not qualitatively [36,50]. Therefore, in this work, we restrict ourselves to the low-energy limit of the Hamiltonian and keep the terms up to the linear order in k. In this regime, the energy dispersion is obtained as

$$E(k) = \pm\sqrt{(\hbar\,v_F\,k\mp V)^2+\Delta^2}, \quad (2)$$

where the first $\pm$ sign refers to the conduction (C) and valance (V) bands, while the sign $\mp$ inside the root square refers to the different branches (1,2) of the (C,V) bands which are separated by the Rashba splitting of the band dispersion.

A schematic figure of the band dispersions is depicted in Fig. 1. In this figure, the horizontal dotted line shows the chemical potential which together with the applied potential V are tunable parameters of the system. As a result of the Rashba splitting, two different Fermi wave vectors, $k_{F1,2}=(\sqrt{\varepsilon_F^2-\Delta^2}\pm V)/\hbar v_F$, appear in the system. Moreover, the red solid lines (the blue dashed lines) show the criteria that the band dispersion comes mostly from the top (bottom) surface [47]. This can be better understood by looking at the Green's function of the system where the local density of states (DOS) of the top surface can be studied separately from the bottom surface and its poles represent the band dispersion. By using $G_0(\mathbf{k},\varepsilon)=[\varepsilon-H_0(\mathbf{k})]^{-1}$, the k-space Green's function

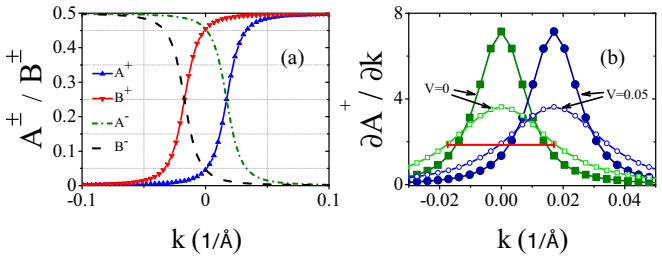

FIG. 2. (a) The weight coefficients $A^{\pm}$ and $B^{\pm}$, as a function of k for $V = 0.05$ eV and $\Delta = 0.035$ eV. (b) Partial derivative of coefficient A^{+} with respect to k for two different potentials, $V = 0, 0.05$ eV, and two different gap sizes, $\Delta = 0.035$ eV (solid symbols) and $\Delta = 0.069$ eV (hollow symbols).

is obtained as

$$G_0(\mathbf{k},\varepsilon) = \begin{bmatrix} g_{t\uparrow t\uparrow} & g_{t\uparrow t\downarrow} & g_{t\uparrow b\uparrow} & g_{t\uparrow b\downarrow} \\ g_{t\downarrow t\uparrow} & g_{t\downarrow t\downarrow} & g_{t\downarrow b\uparrow} & g_{t\downarrow b\downarrow} \\ g_{b\uparrow t\uparrow} & g_{b\uparrow t\downarrow} & g_{b\uparrow b\uparrow} & g_{b\uparrow b\downarrow} \\ g_{b\downarrow t\uparrow} & g_{b\downarrow t\downarrow} & g_{b\downarrow b\uparrow} & g_{b\downarrow b\downarrow} \end{bmatrix}, \tag{3}$$

where $t(b)$ and $\uparrow$ ($\downarrow$) refer to the top (bottom) surface and spin up (down), respectively. In addition, similarities between the components can be considered in this matrix where one has $g_{\downarrow\uparrow} = g^{*}_{\uparrow\downarrow}$ and $g_{\uparrow\uparrow} = g_{\downarrow\downarrow}$. Moreover, all tb components are similar to their corresponding bt components. By focusing on the diagonal elements of the Green's function which are required for calculation of the DOS, we have

$$\begin{aligned} g_{t\uparrow t\uparrow}(k,\varepsilon) &= \frac{A^{+}}{(\varepsilon - E_{V1})} + \frac{A^{-}}{(\varepsilon - E_{C1})} \\ &\quad + \frac{B^{-}}{(\varepsilon - E_{V2})} + \frac{B^{+}}{(\varepsilon - E_{C2})}, \\ g_{b\uparrow b\uparrow}(k,\varepsilon) &= \frac{A^{-}}{(\varepsilon - E_{V1})} + \frac{A^{+}}{(\varepsilon - E_{C1})} \\ &\quad + \frac{B^{+}}{(\varepsilon - E_{V2})} + \frac{B^{-}}{(\varepsilon - E_{C2})}, \end{aligned} \tag{4}$$

where coefficients $A^{\pm}$ and $B^{\pm}$ are functions of k, Δ, and V:

$$\begin{aligned} A^{\pm} &= \frac{\sqrt{\Delta^2 + (k-V)^2} \pm (k-V)}{4\sqrt{\Delta^2 + (k-V)^2}}, \\ B^{\pm} &= \frac{\sqrt{\Delta^2 + (k+V)^2} \pm (k+V)}{4\sqrt{\Delta^2 + (k+V)^2}}. \end{aligned} \tag{5}$$

Using $\mathrm{DOS}(\varepsilon) \propto \frac{-1}{\pi}\sum_k \mathrm{Im}[G(\mathbf{k},\varepsilon)]$ and the fact that the imaginary part of the Green's function is peaked on the poles of Eq. (4) as $\delta(\varepsilon - E(k))$, one can interpret the coefficients $A^{\pm}, B^{\pm}$ as the weight coefficients of the DOS on different band dispersions.

Figure 2(a) shows the behavior of the weight coefficients $A^{\pm}, B^{\pm}$ as a function of k. As shown in this figure, the weight of the conduction band E_{C1} (E_{C2}) at large positive (negative) k is dominated by the bottom (top) surface. At $k = 0$, the dominant contribution of the conduction (valance) band is originated from the top (bottom) surface state. Figure 2(b) shows the k derivative of the coefficient $\frac{\partial A^{+}}{\partial k}$ for different biased potentials, $V = 0, 0.05$ eV, and two different gap sizes, $\Delta = 0.035$ eV (solid symbols) and 0.069 eV (hollow symbols). These diagrams are peaked functions of k with the widths proportional solely to Δ and so the region where the surface states are hybrid with each other depends only on the tunneling between two surfaces.

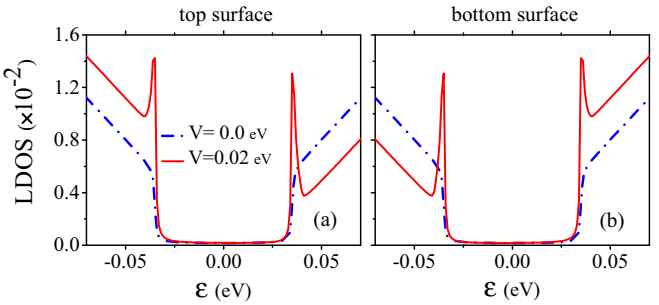

FIG. 3. Illustration of the density of states for an unperturbed system for two different values of voltage, $V = 0$ and $V = 0.02$ eV, for (a) the top and (b) the bottom surfaces.

Figure 3 shows the DOS of different surfaces for fixed tunneling parameter $\Delta = 0.035$ eV and two different values of voltage, $V = 0, 0.02$ eV. As one can see, van Hove singularities appear in the DOS due to the Rashba splitting ($V \neq 0$) when the energy touches the boundaries of the gap, $\varepsilon = \pm\Delta$. The existence of the van Hove singularities near the Fermi energy can drastically enhance the RKKY interaction as has been shown in other materials such as bilayer graphene [8].

B. The RKKY interaction

By placing two magnetic impurities on the surfaces of the TI thin film, the Hamiltonian is modified to

$$H = H_0(\mathbf{k}) + J_c \sum_{i=1,2} S_i \cdot \hat{s}(\mathbf{r}_i), \tag{6}$$

where S_i shows the spin moment of the localized magnetic impurity, $\hat{s}(\mathbf{r}_i) = \hbar/2 \sum_j \sigma_j \delta(\mathbf{r} - \mathbf{r}_j)$ denotes the spin of itinerant electrons, and J_c displays the coupling between them. By applying the second-order perturbation theory, one can transform the interaction between magnetic impurities and itinerant electrons to an indirect exchange interaction between impurities as [1,59,60]

$$H^{\alpha\beta}_{\mathrm{RKKY}} = J_c^2 \sum_{i,j} S^{\alpha}_{1i}\, \chi^{\alpha\beta}_{ij}(r,r')\, S^{\beta}_{2j}, \tag{7}$$

where the spin susceptibility of the system, $\chi^{\alpha\beta}_{ij}(r,r')$, can be evaluated as

$$\begin{aligned} \chi^{\alpha\beta}_{ij}(r,r') &= \frac{-1}{2\pi}\mathrm{Im}\int_{-\infty}^{\varepsilon_F} d\varepsilon \\ &\quad \times \mathrm{Tr}[\sigma_i\, G^{\alpha\beta}(r,r',\varepsilon)\, \sigma_j\, G^{\beta\alpha}(r',r,\varepsilon)]. \end{aligned} \tag{8}$$

Here, α and β denote the t/b surface, $(i,j) = (x,y,z)$ show different directions of the magnetic moment's component, ε_F refers to the Fermi energy, and the trace is taken over the spin degree of freedom.

In order to calculate the spin susceptibility, given by Eq. (8), it is necessary to calculate the unperturbed retarded Green's

function in real space, $G_0^{\rm ret}(\varepsilon,R)$, which reads from the Green's function in k space, given by Eq. (3), by taking the Fourier transformation

$$G_0^{\rm ret}(\varepsilon,R=r_1-r_2)=\frac{1}{\Omega_{BZ}}\int d^2k\, e^{i\,\mathbf{k}\cdot\mathbf{R}}\,G_0(\mathbf{k}). \tag{9}$$

This Green's function has a general form,

$$G_0^{\rm ret}(\varepsilon,\pm R)=\begin{bmatrix} G_{tt} & \mp e^{-i\,\varphi_R}\,G'_{tt} & \vdots & G_{tb} & \mp e^{-i\,\varphi_R}\,G'_{tb} \\ \pm e^{i\,\varphi_R}\,G'_{tt} & G_{tt} & \vdots & \pm e^{i\,\varphi_R}\,G'_{tb} & G_{tb} \\ \cdots & \cdots & \cdots & \cdots & \cdots \\ G_{tb} & \mp e^{-i\,\varphi_R}\,G'_{tb} & \vdots & G_{bb} & \mp e^{-i\,\varphi_R}\,G'_{bb} \\ \pm e^{i\,\varphi_R}\,G'_{tb} & G_{tb} & \vdots & \pm e^{i\,\varphi_R}\,G'_{bb} & G_{bb} \end{bmatrix}, \tag{10}$$

where $\varphi_R=\tan^{-1}(R_y/R_x)$ denotes the polar angle of distance vector $\mathbf{R}$ between impurities. The reader can find the components of the Green's functions in Appendix A.

As mentioned before, we present our results for two situations: the intra- and intersurface cases in which the impurities can be located on the same surface or different surfaces, respectively. For the intrasurface case, we assume the impurities to be located on the top surface and the results of the bottom surface can be achieved by $V\to -V$. After some calculations (see Appendix B), the RKKY Hamiltonian given by Eq. (7) can be written as

$$\begin{aligned} H_{\rm RKKY}=&J_H S_1\cdot S_2+J_I\tilde{S}_1\cdot\tilde{S}_2+\mathbf{J}_{DM}\cdot(\tilde{S}_1\times\tilde{S}_2)\\ &+J_{xy}(\tilde{S}_{1x}\tilde{S}_{2y}+\tilde{S}_{1y}\tilde{S}_{2x}), \end{aligned} \tag{11}$$

where the new spinor $\tilde{S}$ is defined as $\tilde{S}=[S_x\cos(\varphi_R),S_y\sin(\varphi_R),S_z]$, the vector $\mathbf{J}_{DM}=J_{DM}(1,-1,0)$, and $J_{xy}=J_I$. The first term in this equation is similar to the Heisenberg spin interaction which couples the same spin directions with equivalent strength. The second term couples the newly defined spinors $\tilde{S}$, which depends on φ_R and shows the spinor's coupling with different amplitudes in different directions. In the sense that this term favors one direction over the others, it is similar to the Ising interaction and so we call it quasi-Ising-like. These two terms together form an XYZ spin interaction model and will result in collinear alignment of spinors of magnetic impurities S_1 and S_2. Moreover, due to the existence of Rashba spin-orbit coupling in the TI thin film, the symmetry of spin space is broken and so it is expected that the RKKY interaction has terms related to the off-diagonal components of the spin-susceptibility tensor (the third and the fourth terms) [12,13]. While the third term is antisymmetric with respect to the spinors and resembles the Dzyaloshinskii-Moriya (DM) interaction, the last term is symmetric. The existence of two off-diagonal DM terms of xz and yz type together with the last symmetric term J_{xy} can cause the spinors to lie in any plane which provides more tunability in the system. These terms contrarily with the first two terms may cause noncollinear twisted alignment between spinors of impurities, as we will discuss later in Sec. III B.

The RKKY interaction coefficients Js, introduced in Eq. (11), are defined as follows for the intrasurface (tt) and intersurface (tb) cases:

$$\begin{aligned} J_H^{tt/tb}&=-\frac{1}{\pi}{\rm Im}\int_{-\infty}^{\varepsilon_F}d\varepsilon\,\left[G^2_{tt/tb}(\varepsilon,R)+G'^2_{tt/tb}(\varepsilon,R)\right],\\ J_I^{tt/tb}&=\frac{2}{\pi}{\rm Im}\int_{-\infty}^{\varepsilon_F}d\varepsilon\,G'^2_{tt/tb}(\varepsilon,R),\\ J_{DM}^{tt/tb}&=-\frac{2}{\pi}{\rm Im}\int_{-\infty}^{\varepsilon_F}d\varepsilon\,G_{tt/tb}(\varepsilon,R)\,G'_{tt/tb}(\varepsilon,R). \end{aligned} \tag{12}$$

In conventional two-dimensional materials with isotropic band dispersion, the RKKY interaction does not depend on the direction of $\mathbf{R}$. Provided in systems with Rashba spin-orbit coupling, the spin of itinerant electrons is coupled to the wave vector $\mathbf{k}$ and the in-plane component of the impurity's magnetic moment breaks the isotropy of the system. As a result, the spin response $\chi_{ij}(\mathbf{R})$ depends both on the magnitude and direction of the vector $\mathbf{R}$ [55,56].

Figure 4 shows the angle dependency of the spin susceptibility. Here, we have assumed both impurities to be located on the top surface and $\varepsilon_F=0.135$ eV, $\Delta=0.035$ eV, and (a),(b) $V=0$ and (c),(d) $V=0.02$ eV. We have plotted diagonal

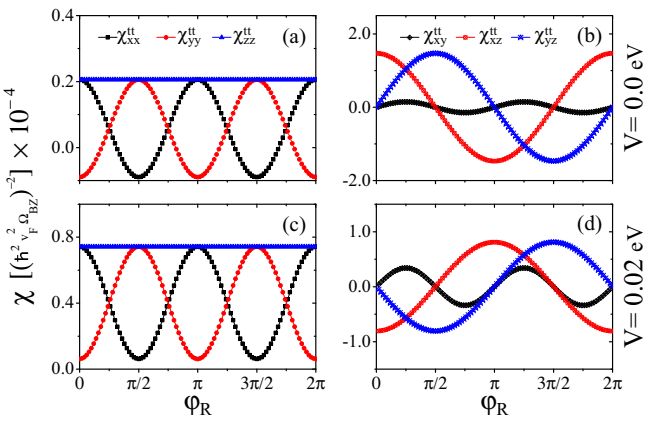

FIG. 4. The (a),(c) diagonal and (b),(d) off-diagonal components of susceptibility tensor $\chi_{ij}^{\alpha\beta}$ as a function of polar angle φ_R are showed for the intrasurface case. All of them are scaled by $(\frac{1}{\hbar^2 v_F^2\Omega_{BZ}})^2$. Here, we set to $\Delta=0.035$ eV, $\varepsilon_F=0.135$ eV, $R=30$ nm, $v_F=4.48\times 10^5\,\frac{m}{s}$, and (a),(b) $V=0$ eV and (c),(d) $V=0.02$ eV.

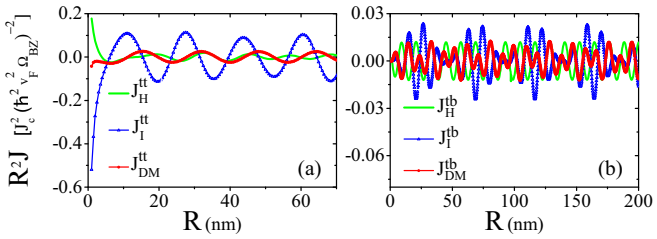

FIG. 5. The RKKY interaction terms times R^2 ($R^2 J_i^{\alpha\beta}$ for $i = H, I, DM$), as a function of the distance in units of nm, scaled by $(\frac{J_c}{\hbar^2 v_F^2 \Omega_{BZ}})^2$. Here we set $\Delta = 0.035$ eV, $V = 0.02$ eV, $\varepsilon_F = 0.085$ eV, and $v_F = 4.48 \times 10^5 \frac{m}{s}$. (a) and (b) refer to the intra- and intersurface cases, respectively.

parts of the spin-susceptibility tensor in Figs. 4(a) and 4(c) and off-diagonal parts in Figs. 4(b) and 4(d). While diagonal terms oscillate with $2\varphi_R$ (except χ_{zz}, which is angle independent), the off-diagonal terms oscillate with φ_R as expected from Eq. (B1). Besides, by comparing the upper and lower panels, it is clear how applying a voltage can drastically change the sign and magnitude of the interaction terms.

III. RESULTS AND DISCUSSIONS

In this section, we present our results for the RKKY interaction between two magnetic impurities located on the top surface (tt) or on two different surfaces (tb).

The behavior of the RKKY interaction terms is severely affected by the distance between two magnetic impurities. In two-dimensional materials, they usually fall off with R^{-2} and oscillate as $\sim \sin(2k_F R)$; however, for multiband materials, a more complicated behavior is expected. In Fig. 5, we have plotted J_H, J_I, J_{DM}, times R^2, scaled by $(\frac{J_c}{\hbar^2 v_F^2 \Omega_{BZ}})^2$, in terms of distance R for the intrasurface [Fig. 5(a)] and intersurface [Fig. 5(b)] cases. As one can see, all interaction terms decay as R^{-2} for the long-range distances, like the other two-dimensional structures [4,13]. For the intrasurface pairing, the RKKY interaction takes much higher values in the short-distance limit, which plays a more prominent role at higher densities of impurities. Although there exist two Fermi wave vectors in the system due to finite value of V, based on our previous discussion on the weight coefficients given by Eq. (5), the top surface's electrons mostly come with k_{F2} and so the RKKY interaction oscillates approximately sinusoidal. In contrast to this case, the RKKY interaction for intersurface pairing is mediated by both surface's electrons and the existence of two Fermi wave vectors in the system results in a beating-type pattern, as shown in Fig. 5(b). Moreover, it is worthwhile to mention that unlike the intrasurface case, the RKKY interaction starts from nearly zero values at short distances for impurities on different surfaces and also the magnitude of this coupling is one order of magnitude smaller than intra+surface coupling.

In Fig. 6, the behavior of all RKKY interaction terms as a function of R has been shown for two critical Fermi energies: the Fermi energy at the edge of the gap ($\varepsilon_F = \Delta$) [Figs. 6(a) and 6(b)] and the Fermi energy in which k_{F2} becomes zero [Figs. 6(c) and 6(d)]. Here, we set $\Delta = 0.035$ eV

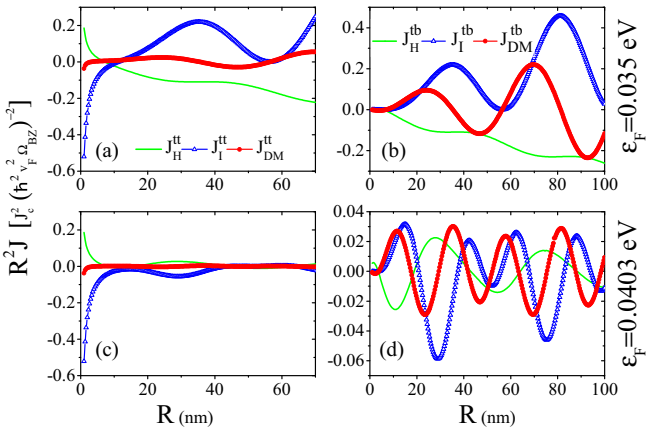

FIG. 6. The RKKY interaction terms ($J_i^{\alpha\beta}$ for $i = H, I, DM$), scaled by $(\frac{J_c}{\hbar^2 v_F^2 \Omega_{BZ}})^2$, as a function of distance for two cases: $\varepsilon_F = 0.035$ and $\varepsilon_F = 0.0403$ eV. Here we set $V = 0.02$ eV, $\Delta = 0.035$ eV, and $v_F = 4.48 \times 10^5 \frac{m}{s}$. (a),(c) Intrasurface and (b),(d) intersurface cases, respectively.

and $V = 0.02$ eV. For the case in which the Fermi energy lies at the edge of the band gap [Figs. 6(a) and 6(b)], where van Hove singularities occur (see Fig. 3), the magnitude of all RKKY interaction terms notably increases and they decay slower than R^{-2}. For the other special Fermi energy, $\varepsilon_F = 0.0403$ eV, for which $k_{F2} = 0$, since the electrons with k_{F2} mostly come from the top surface, there would remain no Fermi electron to mediate the intrasurface RKKY interaction and so it becomes more short range and takes smaller values in comparison with Fig. 5(a). However, in the case of intersurface pairing, the RKKY interaction roughly obeys the R^{-2} decay rule, but the previous beating-type oscillation [Fig. 5(b)] disappears due to the existence of only one k_F in the system.

Figure 7 shows the effect of the Fermi energy on the RKKY interaction terms for intrasurface [Figs. 7(a) and 7(c)] and intersurface [Figs. 7(b) and 7(d)] pairing. Here, we choose $R = 30$ nm, $\Delta = 0.035$ eV, and also $V = 0$ eV

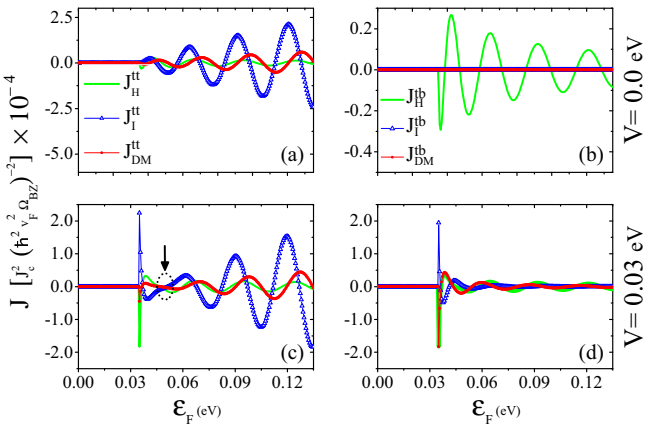

FIG. 7. The (a),(c) intrasurface and (b),(d) intersurface RKKY interaction couplings ($J_i^{\alpha\beta}$ for $i = H, I, DM$), scaled by $(\frac{J_c}{\hbar^2 v_F^2 \Omega_{BZ}})^2$, as a function of the Fermi energy in units of eV. Here we set $\Delta = 0.035$ eV, $R = 30$ nm, $v_F = 4.48 \times 10^5 \frac{m}{s}$, and (a),(b) $V = 0$ eV and (c),(d) $V = 0.03$ eV.

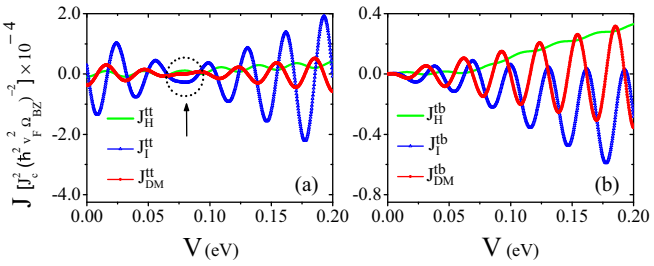

FIG. 8. The RKKY interaction terms ($J_i^{\alpha\beta}$ for $i = H, I, DM$), scaled by $(\frac{J_c}{\hbar^2 v_F^2 \Omega_{BZ}})^2$, as a function of voltage. Here we set $R = 30$ nm, $\Delta = 0.035$ eV, $\varepsilon_F = 0.085$ eV, and $v_F = 4.48 \times 10^5 \frac{m}{s}$. (a) and (b) refer to the intra- and intersurface cases, respectively.

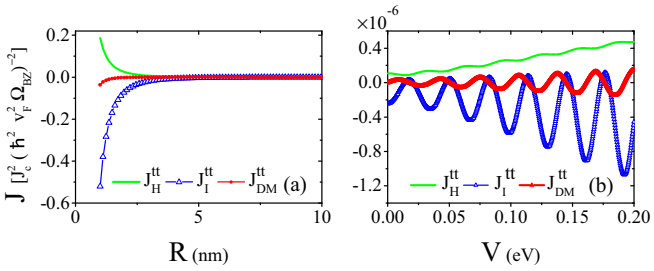

FIG. 9. The van Vleck interaction terms ($J_i^{\alpha\beta}$ for $i = H, I, DM$), scaled by $(\frac{J_c}{\hbar^2 v_F^2 \Omega_{BZ}})^2$, as a function of (a) distance and (b) voltage. Here we set $\Delta = 0.035$ eV, $\varepsilon_F = 0.0$ eV, and $v_F = 4.48 \times 10^5 \frac{m}{s}$, and (a) $V = 0.02$ eV and (b) $R = 30$ nm.

[Figs. 7(a) and 7(b)] and $V = 0.05$ eV [Figs. 7(c) and 7(d)]. As shown in these figures, for the Fermi energies inside the gap, $\varepsilon_F < \Delta$, considering the insulating nature of the material, all terms of the interactions are very small but finite according to the van Vleck mechanism [32,36]. In the finite doping region $\varepsilon_F > \Delta$, different behavior is seen between intra- and intersurface pairings. While for the intrasurface case and $V = 0$, the oscillation's amplitude of the RKKY interaction terms gradually increases with the Fermi energy according to the increase of the DOS [Fig. 7(a)], for the intersurface case, based on the weight coefficient discussion, the hybridization among different surfaces decreases so the intersurface RKKY coupling decays with energy [Fig. 7(b)]. Moreover, in this case, one can see that only the Heisenberg-like coupling appears and all other terms are zero. As mentioned before, the existence of Ising-like and DM-like terms is related to the breaking of spin degeneracy of the system. However, in the case of intersurface coupling with inversion symmetry between surfaces at $V = 0$, the bands belonging to different spin helical states will not be split. Since the coupling term Δ is spin independent, the RKKY interaction becomes an isotropic collinear Heisenberg-like term. For $V \neq 0$, as a result of the van Hove singularities at the edge of the band gap, the RKKY interaction takes very large values at very small doping [Figs. 7(c) and 7(d)]. In the presence of Rashba splitting, shown in Fig. 7(c), first, all terms fall off by the decrease of k_{F2} and then, after the critical Fermi energy $\varepsilon_F = \sqrt{V^2 + \Delta^2}$ where $k_{F2} = 0$, they increase. In contrast to Fig. 7(b), breaking structural inversion symmetry, $V \neq 0$ [Fig. 7(d)], and the Rashba splitting causes other types of couplings to reappear in the intersurface coupling.

It is worthwhile to mention that by splitting Eq. (8) into two integrals as $\int_{-\infty}^{0} + \int_{0}^{\varepsilon_F}$, one can see that the RKKY interaction comes from all electrons in the system including the valance-band ones; however, since the van Vleck interaction [Fig. 9(b)] is about three orders of magnitude smaller than the RKKY interaction [Fig. 8(a)], one can conclude that the RKKY interaction comes mostly from the Fermi electrons. Moreover, in a quick look at Eq. (8), the susceptibility is proportional to the imaginary part of the Green's function multiplication, $\mathrm{Im}(GG)$, which can be divided into $\mathrm{Im}(G)\mathrm{Re}(G)$. It means that both the DOS $\propto \mathrm{Im}(G)$ and $\mathrm{Re}(G)$ play a role in the susceptibility. At energies with van Hove singularity, the imaginary part of the Green's function is drastically enhanced and since the RKKY interaction comes mostly from the Fermi electrons, it increases as the Fermi energy touches the van Hove points.

To study the effect of Rashba splitting on the RKKY interaction, in Fig. 8, we show the behavior of all terms with respect to V for intrasurface [Fig. 8(a)] and intersurface [Fig. 8(b)] pairing. By fixing the chemical potential and varying the applied bias, one can tune the Fermi wave vectors and, as a consequence, the RKKY interaction. Manipulating the magnetic properties of materials with electric field is very desirable for spintronic technologies [61]. For the intrasurface pairing depicted in Fig. 8(a), the RKKY interaction drops by a decrease of k_{F2} and then, after the critical biased voltage, $V = \sqrt{\varepsilon_F^2 - \Delta^2}$ in which $k_{F2} = 0$, it increases. At this critical voltage, similar to what happens at the critical Fermi energy [Fig. 7(c)], the density of electrons on the top surface that mediates the coupling among magnetic impurities becomes nearly zero and the RKKY strength gets its minimum (the black dashed circle). For the intersurface case, both k_Fs play a role and the interaction increases.

A. van Vleck interaction

The RKKY interaction refers to the indirect exchange interaction via the conduction's electrons which occur in the metallic phase of systems. However, paying attention to Eq. (8) reveals that the RKKY interaction is originated from all energies lower than the Fermi energy ε_F as well, so it has nonzero value even at zero chemical doping $\varepsilon_F = 0$. Although in this regime the indirect exchange coupling known as the van Vleck interaction is much weaker than the RKKY, it can affect magnetic phases of materials as well [36]. The zz component of the van Vleck interaction (related to χ_{zz}) has been studied in TI thin films [36] to describe the ferromagnetic phase in the QAHE experiment. Here, we investigate all terms of this interaction and their tunability with the biased potential V.

Figure 9(a) shows the van Vleck interaction as a function of the distance R. As shown in this figure, all interaction terms fall off very rapidly and become zero after $R \sim 3$ nm. Figure 9(b) shows how this interaction is also oscillating with the biased electric potential V. Moreover, it is obvious that V makes the van Vleck interaction stronger.

B. Rotation of spinors

The off-diagonal components of the spin-susceptibility tensor, $\chi_{ij}, i \neq j$, couple different spin direction of impurities and so can rotate the impurity's spinors with respect to each other [4], which results in chiral magnetization in multi-impurity systems [62]. In this part, we discuss the difference between symmetric and antisymmetric terms of the RKKY interaction in the rotation of impurities. We suppose two RKKY model Hamiltonians both including a Heisenberg-like term together with an Ising-like term, in addition to [model $M1$ ($M2$)] a symmetric (antisymmetric) coupling,

$$\begin{aligned} M1: H &= J_H \mathbf{S}_1 \cdot \mathbf{S}_2 + J_I \mathbf{S}_{1z}\mathbf{S}_{1z} + J_{DM}(\mathbf{S}_{1x}\mathbf{S}_{2y} - \mathbf{S}_{1y}\mathbf{S}_{2x}), \\ M2: H &= J_H \mathbf{S}_1 \cdot \mathbf{S}_2 + J_I \mathbf{S}_{1z}\mathbf{S}_{1z} + J_{XY}(\mathbf{S}_{1x}\mathbf{S}_{2y} + \mathbf{S}_{1y}\mathbf{S}_{2x}). \end{aligned} \tag{13}$$

By assuming S_1 and S_2 as classical vectors, we can write them in the form of $S_{i=1,2} = |S_i|\,(\sin\theta_i \cos\varphi_i, \sin\theta_i \cos\varphi_i, \cos\theta_i)$, so the Hamiltonian is rewritten as

$$\begin{aligned} M1: H_{\mathrm{RKKY}} &= |S_1|\,|S_2|\,[(J_H + J_I)\cos\theta_1\ \cos\theta_2 \\ &\quad + \sin\theta_1\ \sin\theta_2(J_H \cos\varphi_- + J_{DM}\sin\varphi_-)], \\ M2: H_{\mathrm{RKKY}} &= |S_1|\,|S_2|\,[(J_H + J_I)\cos\theta_1\ \cos\theta_2 \\ &\quad + \sin\theta_1\ \sin\theta_2(J_H \cos\varphi_- + J_{XY}\sin\varphi_+)], \end{aligned} \tag{14}$$

where $\varphi_\pm = \varphi_1 \pm \varphi_2$. Note that in the first model, including antisymmetric term J_{DM}, the Hamiltonian can be expressed as a function of $\varphi_1 - \varphi_2$, while in the model $M2$, both φ_1 and φ_2 are important.

To find the minimum energy and configuration of the spinors, we should set $\frac{\partial H}{\partial \theta_{1,2}} = 0$ and $\frac{\partial H}{\partial \varphi_{1,2}} = 0$, where the first relation binds (θ_1,θ_2) to be (0,0), (0,π), (π,0), (π,π), and ($\pi/2$,$\pi/2$). The only possibility of the rotated spinors is $\theta_{1,2} = \pi/2$, in which the values of $\varphi_{1,2}$ are meaningful. For the first model $M1$, by setting $\frac{\partial H}{\partial \varphi_-} = 0$, we obtain

$$\frac{\partial H}{\partial \varphi_-} = -J_H \sin\varphi_- + J_{DM}\cos\varphi_- = 0 \Rightarrow \tan\varphi_- = \frac{J_{DM}}{J_H}. \tag{15}$$

Calculating $\frac{\partial H}{\partial \varphi_{1,2}} = 0$ in the model $M2$ results in different possibilities: $\varphi_1 = \varphi_2$, $\varphi_1 = \varphi_2 + \pi$, $\varphi_1 = \pi/2 - \varphi_2$, or $\varphi_1 = 3\pi/2 - \varphi_2$. So while in the first model any rotation angle is basically possible for impurities, in the second one they can be aligned ferro- or antiferromagnetically, or with a $\pi/2$ rotation with respect to each other.

IV. SUMMARY AND DISCUSSION

In summary, we investigate the effect of Rashba-type band splitting on the RKKY interaction in topological-insulator thin films. We have derived the RKKY interaction for magnetic impurities considering both intersurface and intrasurface interactions, where the results show completely different behavior. These diverse behaviors are described by mapping the density of states onto the band dispersion and determining the weight coefficient of each band in the DOS. Moreover, we demonstrated that the RKKY interaction in the Rashba materials has a strong direction dependency (spatial anisotropy) when at least one of the impurities has an in-plane spin component. In addition to the conventional RKKY interaction terms mentioned in the Rashba materials, namely Heisenberg-like, Ising-like, and DM-like terms, we found another term of the spin-susceptibility tensor, which in contrast to the DM term is symmetric under the interchange of impurities. At zero chemical potential, for the interaction usually known as the van Vleck mechanism, we show how one can enhance the exchange interaction using the perpendicular electric field. This study sheds light on solving the problem of the QAHE, which has been done experimentally at zero chemical doping. Furthermore, it is shown that the Rashba splitting causes the existence of van Hove singularities in the gap edge of the band dispersion, which give rise to large values of the RKKY interaction. As a result of a small value of chemical doping, the RKKY interaction can be extremely modified.

ACKNOWLEDGMENTS

F.P. thanks M. Pereiro, A. Qaiumzadeh, M. Mashkoori, and K. Björnson for useful discussions. M.Sh. thanks S. Amiri for his supportive role and also acknowledges the Institute for Research in Fundamental Sciences (IPM) for their hospitality. H.C. acknowledges the International Center for Theoretical Physics (ICTP) for hospitality and support in capacity of Regular Associate program of the center.

APPENDIX A: DETAILS OF GREEN'S FUNCTION

Taking the integrals of Eq. (9) according to the Fourier transformation gives rise to the Green's function in real space. Using two-dimensional polar coordination in k space, we have $\exp(i\,\mathbf{k}\cdot\mathbf{R}) = \exp[i\,k\,R\,\cos(\varphi_k - \varphi_R)]$ and so $G_0^{\mathrm{ret}}(\varepsilon, \pm R)$ [Eq. (10)] components are obtained as the following:

$$\begin{aligned} G_{tt}(\varepsilon,R) &= -2\pi\alpha \sum_{s=\pm} a_{-s}(\gamma - isV)K_0^s, \quad G'_{tt}(\varepsilon,R) = -2\pi i\alpha \sum_{s=\pm} \frac{s a_{-s}}{\sqrt{\frac{-1}{(V+is\gamma)^2}}} K_1^s, \\ G_{tb}(\varepsilon,R) &= \pi i\alpha \frac{\Delta}{\gamma} \sum_{s=\pm} s(V + is\gamma)K_0^s, \quad G'_{tb}(\varepsilon,R) = -\pi i\alpha \frac{\Delta}{\gamma} \sum_{s=\pm} \frac{s}{\sqrt{\frac{-1}{(V+is\gamma)^2}}} K_1^s, \\ G_{bb}(\varepsilon,R) &= -2\pi\alpha \sum_{s=\pm} a_s(\gamma - isV)K_0^s, \quad G'_{bb}(\varepsilon,R) = -2\pi i\alpha \sum_{s=\pm} \frac{s a_s}{\sqrt{\frac{-1}{(V+is\gamma)^2}}} K_1^s, \end{aligned} \tag{A1}$$

where $\alpha = 1/\hbar^2 v_F^2 \Omega_{BZ}$, $\gamma = \sqrt{\Delta^2 - \varepsilon^2}$, and for $s = \pm$, $a_s = \frac{1}{2}(\frac{\varepsilon}{\gamma} + si)$, whereas $K^s_{0/1}$ are the zeroth and first order of the modified Bessel functions of the second kind:

$$K_0^s = K_0\left(\frac{R}{\sqrt{-\frac{\hbar^2 v_F^2}{(V+si\gamma)^2}}}\right), \quad K_1^s = K_1\left(\frac{R}{\sqrt{-\frac{\hbar^2 v_F^2}{(V-si\gamma)^2}}}\right). \tag{A2}$$

APPENDIX B: CALCULATION OF THE RKKY HAMILTONIAN

The spin susceptibility can be rewritten as $\chi_{ij}^{\alpha\beta} = \frac{-1}{2\pi}\mathrm{Im}\int_{-\infty}^{\varepsilon_F} d\varepsilon F_{ij}^{\alpha\beta}$, where $F_{ij}^{\alpha\beta} = \mathrm{Tr}[\sigma_i\ G^{\alpha\beta}(r,r',\varepsilon)\ \sigma_j\ G^{\beta\alpha}(r',r,\varepsilon)]$ for the intrasurface case ($\alpha\beta = tt$) and intersurface case ($\alpha\beta = tb$) given by

$$\begin{aligned}
F_{xx}^{tt(tb)} &= 2\big[G_{tt(tb)}^2 - G_{tt(tb)}^{'2}\ \cos(2\varphi_R)\big],\\
F_{yy}^{tt(tb)} &= 2\big[G_{tt(tb)}^2 + G_{tt(tb)}^{'2}\ \cos(2\varphi_R)\big],\\
F_{zz}^{tt(tb)} &= 2\ \big(G_{tt(tb)}^2 - G_{tt(tb)}^{'2}\big),\\
F_{xy}^{tt(tb)} &= F_{yx}^{tt(tb)} = -2\ G_{tt(tb)}^{'2}\ \sin(2\varphi_R),\\
F_{xz}^{tt(tb)} &= -F_{zx}^{tt(tb)} = 4\ G_{tt(tb)}\ G'_{tt(tb)}\ \cos(\varphi_R),\\
F_{yz}^{tt(b)} &= -F_{zy}^{tt(b)} = 4\ G_{tt(tb)}\ G'_{tt(tb)}\ \sin(\varphi_R).
\end{aligned} \tag{B1}$$

By inserting the above relations in Eq. (7), the RKKY Hamiltonian is achieved:

$$\begin{aligned}
H_{\mathrm{RKKY}}^{\alpha\beta} &= \frac{-J_c^2}{2\pi}\mathrm{Im}\int_{-\infty}^{\varepsilon_F} d\varepsilon \mathrm{Tr}\left[\sum_{i,j} S_{1i}^{\alpha}\ \chi_{ij}^{\alpha\beta}(r,r')\ S_{2j}^{\beta}\right]\\
&= \frac{-J_c^2}{2\pi}\mathrm{Im}\int_{-\infty}^{\varepsilon_F} d\varepsilon \mathrm{Tr}\big[S_{1x}^{\alpha}\ F_{xx}^{\alpha\beta}\ S_{2x}^{\beta} + S_{1y}^{\alpha}\ F_{yy}^{\alpha\beta}\ S_{2y}^{\beta} + S_{1z}^{\alpha}\ F_{zz}^{\alpha\beta}\ S_{2z}^{\beta} + S_{1x}^{\alpha}\ F_{xy}^{\alpha\beta}\ S_{2y}^{\beta}\\
&\quad + S_{1y}^{\alpha}\ F_{yx}^{\alpha\beta}\ S_{2x}^{\beta} + S_{1x}^{\alpha}\ F_{xz}^{\alpha\beta}\ S_{2z}^{\beta} + S_{1z}^{\alpha}\ F_{zx}^{\alpha\beta}\ S_{2x}^{\beta} + S_{1y}^{\alpha}\ F_{yz}^{\alpha\beta}\ S_{2z}^{\beta} + S_{1z}^{\alpha}\ F_{zy}^{\alpha\beta}\ S_{2y}^{\beta}\big],
\end{aligned} \tag{B2}$$

$$\begin{aligned}
H_{\mathrm{RKKY}}^{\alpha\beta} = \frac{-J_c^2}{\pi}\mathrm{Im}\int_{-\infty}^{\varepsilon_F} d\varepsilon \mathrm{Tr}\big[&S_{1x}^{\alpha}\ S_{2x}^{\beta}\big[G_{\alpha\beta}^2 - G_{\alpha\beta}^{'2}\ \cos(2\varphi_R)\big] + S_{1y}^{\alpha}\ S_{2y}^{\beta}\big[G_{\alpha\beta}^2 + G_{\alpha\beta}^{'2}\ \cos(2\varphi_R)\big] + S_{1z}^{\alpha}\ S_{2z}^{\beta}\big(G_{\alpha\beta}^2 - G_{\alpha\beta}^{'2}\big)\\
&- \big(S_{1x}^{\alpha}\ S_{2y}^{\beta} + S_{1y}^{\alpha}\ S_{2x}^{\beta}\big)G_{\alpha\beta}^{'2}\sin(2\varphi_R) + 2\big(S_{1x}^{\alpha}\ S_{2z}^{\beta} - S_{1z}^{\alpha}\ S_{2x}^{\beta}\big)\ G_{\alpha\beta}\ G_{\alpha\beta}^{'}\cos(\varphi_R)\\
&+ 2\big(S_{1y}^{\alpha}\ S_{2z}^{\beta} - S_{1z}^{\alpha}\ S_{2y}^{\beta}\big)\ G_{\alpha\beta}\ G_{\alpha\beta}^{'}\sin(\varphi_R)\big].
\end{aligned} \tag{B3}$$

Now, by using trigonometry relations $\cos(2\varphi_R) = 2\cos^2(\varphi_R) - 1$ and $\cos(2\varphi_R) = 1 - 2\sin^2(\varphi_R)$, the RKKY Hamiltonian is of the form

$$\begin{aligned}
H_{\mathrm{RKKY}}^{\alpha\beta} = \frac{-J_c^2}{\pi}\mathrm{Im}\int_{-\infty}^{\varepsilon_F} d\varepsilon\ \mathrm{Tr}\big(&S_{1x}^{\alpha}\ S_{2x}^{\beta}\big\{G_{\alpha\beta}^2 - G_{\alpha\beta}^{'2}[2\cos(\varphi_R) - 1]\big\} + S_{1y}^{\alpha}\ S_{2y}^{\beta}\big\{G_{\alpha\beta}^2 + G_{\alpha\beta}^{'2}\ [1 - 2\sin(\varphi_R)]\big\} + S_{1z}^{\alpha}\ S_{2z}^{\beta}\\
&\big(G_{\alpha\beta}^2 + G_{\alpha\beta}^{'2} - 2G_{\alpha\beta}^{'2}\big) - 2\big(S_{1x}^{\alpha}\ S_{2y}^{\beta} + S_{1y}^{\alpha}\ S_{2x}^{\beta}\big)G_{\alpha\beta}^{'2}\sin(\varphi_R)\cos(\varphi_R) + 2\big(S_{1x}^{\alpha}\ S_{2z}^{\beta} - S_{1z}^{\alpha}\ S_{2x}^{\beta}\big)G_{\alpha\beta}G_{\alpha\beta}^{'}\cos(\varphi_R)\\
&\times + 2\big(S_{1y}^{\alpha}\ S_{2z}^{\beta} - S_{1z}^{\alpha}\ S_{2y}^{\beta}\big)\ G_{\alpha\beta}\ G_{\alpha\beta}^{'}\sin(\varphi_R)\big).
\end{aligned} \tag{B4}$$

By introducing new spinors $\tilde{S} = [S_x\cos(\varphi_R), S_y\sin(\varphi_R), S_z]$, with $\varphi_R = \tan^{-1}(R_y/R_x)$, we have

$$\begin{aligned}
H_{\mathrm{RKKY}}^{\alpha\beta} = \frac{-J_c^2}{\pi}\mathrm{Im}\int_{-\infty}^{\varepsilon_F} d\varepsilon \mathrm{Tr}\big\{&\big(G_{\alpha\beta}^2 + G_{\alpha\beta}^{'2}\big)S_1\cdot S_2 - 2\ G_{\alpha\beta}^{'2}\tilde{S}_1\cdot\tilde{S}_2 - 2\ G_{\alpha\beta}^{'}(\tilde{S}_{1x}\ \tilde{S}_{2y} + \tilde{S}_{1y}\ \tilde{S}_{2x})\\
&+ 2G_{\alpha\beta}\ G_{\alpha\beta}^{'}[(\tilde{S}_1\times\tilde{S}_2)_x - (\tilde{S}_1\times\tilde{S}_2)_y]\big\}.
\end{aligned} \tag{B5}$$

Finally, the RKKY Hamiltonian can be obtained as the compact form given in Eq. (11).

[1] M. A. Ruderman and C. Kittel, Phys. Rev. **96**, 99 (1954).

[2] T. Kasuya, Prog. Theor. Phys. **16**, 45 (1956).

[3] K. Yosida, Phys. Rev. **106**, 893 (1957).
[4] F. Parhizgar, H. Rostami, and R. Asgari, Phys. Rev. B **87**, 125401 (2013).
[5] F. Parhizgar, R. Asgari, S. H. Abedinpour, and M. Zareyan, Phys. Rev. B **87**, 125402 (2013).
[6] M. Sherafati and S. Satpathy, Phys. Rev. B **83**, 165425 (2011).
[7] A. M. Black-Schaffer, Phys. Rev. B **81**, 205416 (2010).
[8] F. Parhizgar, M. Sherafati, R. Asgari, and S. Satpathy, Phys. Rev. B **87**, 165429 (2013).
[9] K. Szalowski, Phys. Rev. B **84**, 205409 (2011).
[10] M. M. Valizadeh, Int. J. Mod. Phys. B **30**, 1650234 (2016).
[11] M. M. Valizadeh and S. Satpathy, Int. J. Mod. Phys. B. **29**, 1550219 (2015); Physica Status Solidi **253**, 2245 (2016).
[12] H. Imamura, P. Bruno, and Y. Utsumi, Phys. Rev. B **69**, 121303(R) (2004).
[13] J.-J. Zhu, D.-X. Yao, S.-C. Zhang, and K. Chang, Phys. Rev. Lett. **106**, 097201 (2011).
[14] D. A. Abanin and D. A. Pesin, Phys. Rev. Lett. **106**, 136802 (2011).
[15] M. Zare, F. Parhizgar, and R. Asgari, Phys. Rev. B **94**, 045443 (2016).
[16] J. Klinovaja and D. Loss, Phys. Rev. B **87**, 045422 (2013).
[17] I. E. Dzialoshinskii *et al.*, JETP **5**, 1259 (1957).
[18] V. E. Dmitrienko *et al.*, JETP Lett. **92**, 383 (2010).
[19] A. T. Hindmarch and B. J. Hickey, Phys. Rev. Lett. **91**, 116601 (2003).
[20] A. A. Khajetoorians *et al.*, Nat. Phys. **8**, 497 (2012).
[21] L. Zhou *et al.*, Nat. Phys. **6**, 187 (2010).
[22] S. R. Power and M. S. Ferreira, Crystals **3**, 49 (2013).
[23] K. Szalowski and T. Balcerzak, Phys. Rev. B **77**, 115204 (2008).
[24] E. H. Hwang and S. Das Sarma, Phys. Rev. Lett. **101**, 156802 (2008).
[25] D. J. Priour, Jr., E. H. Hwang, and S. Das Sarma, Phys. Rev. Lett. **92**, 117201 (2004).
[26] F. Matsukura, H. Ohno, A. Shen, and Y. Sugawara, Phys. Rev. B **57**, R2037(R) (1998).
[27] K.-T. Ko *et al.*, Phys. Rev. Lett. **107**, 247201 (2011).
[28] H. Ohno, Science **281**, 951 (1998).
[29] P. J. T. Eggenkamp, H. J. M. Swagten, T. Story, V. I. Litvinov, C. H. W. Swüste, and W. J. M. de Jonge, Phys. Rev. B **51**, 15250 (1995).
[30] F.-s. Liu, W. A. Roshen, and J. Ruvalds, Phys. Rev. B **36**, 492 (1987).
[31] M. H. Christensen, M. Schecter, K. Flensberg, B. M. Andersen, and J. Paaske, Phys. Rev. B **94**, 144509 (2016).
[32] R. Yu *et al.*, Science **329**, 61 (2010).
[33] C.-Z. Chang *et al.*, Science **340**, 167 (2013).
[34] X. Kou, S. T. Guo, Y. Fan, L. Pan, M. Lang, Y. Jiang, Q. Shao, T. Nie, K. Murata, J. Tang, Y. Wang, L. He, T. K. Lee, W. L. Lee, and K. L. Wang, Phys. Rev. Lett. **113**, 137201 (2014).
[35] J. G. Checkelsky *et al.*, Nat. Phys. **10**, 731 (2014).
[36] J. Wang, B. Lian, and S.-C. Zhang, Phys. Rev. Lett. **115**, 036805 (2015).
[37] T. R. F. Peixoto, H. Bentmann, S. Schreyeck, M. Winnerlein, C. Seibel, H. Maass, M. Al-Baidhani, K. Treiber, S. Schatz, S. Grauer, C. Gould, K. Brunner, A. Ernst, L. W. Molenkamp, and F. Reinert, Phys. Rev. B **94**, 195140 (2016).
[38] M. Z. Hasan and C. L. Kane, Rev. Mod. Phys. **82**, 3045 (2010).
[39] X.-L. Qi and S.-C. Zhang, Rev. Mod. Phys. **83**, 1057 (2011).
[40] J. E. Moore, Nature (London) **464**, 194 (2010).
[41] H. Zhang, C.-X. Liu, X.-L. Qi, X. Dai, Z. Fang, and S.-C. Zhang, Nat. Phys. **5**, 438 (2009).
[42] Y. Zhang *et al.*, Nat. Phys. **6**, 584 (2010).
[43] T. O. Wehling, A. M. Black-Schaffer, and A. V. Balatsky, Adv. Phys. **63**, 1 (2014).
[44] D. Pesin and A. H. MacDonald, Nat. Mater. **11**, 409 (2012).
[45] J. Linder, T. Yokoyama, and A. Sudbo, Phys. Rev. B **80**, 205401 (2009).
[46] C.-X. Liu, H. J. Zhang, B. Yan, X.-L. Qi, T. Frauenheim, X. Dai, Z. Fang, and S.-C. Zhang, Phys. Rev. B **81**, 041307(R) (2010).
[47] W.-Y. Shan, H.-Z. Lu, and S.-Q. Shen, New J. Phys. **12**, 043048 (2010).
[48] F. Parhizgar and A. M. Black-Schaffer, arXiv:1609.01038v1.
[49] F. Parhizgar and A. M. Black-Schaffer, Phys. Rev. B **90**, 184517 (2014).
[50] F. Parhizgar, A. G. Moghaddam, and R. Asgari, Phys. Rev. B **92**, 045429 (2015).
[51] P. Sessi, F. Reis, T. Bathon1, K. A. Kokh O. E. Tereshchenko, and M. Bode, Nat. Commun. **5**, 5349 (2014).
[52] L. A. Wray *et al.*, Nat. Phys. **7**, 32 (2010).
[53] P. Stano, J. Klinovaja, A. Yacoby, and D. Loss, Phys. Rev. B **88**, 045441 (2013).
[54] A. A. Zyuzin and D. Loss, Phys. Rev. B **90**, 125443 (2014).
[55] D. K. Efimkin and V. Galitski, Phys. Rev. B **89**, 115431 (2014).
[56] Y. W. Lee and Y. L. Lee, Phys. Rev. B **91**, 214431 (2015).
[57] Q. Liu, C.-X. Liu, C. Xu, X.-L. Qi, and S.-C. Zhang, Phys. Rev. Lett. **102**, 156603 (2009).
[58] S. S. Pershoguba and V. M. Yakovenko, Phys. Rev. B **86**, 165404 (2012).
[59] G. Grosso and G. P. Parravicini, *Solid State Physics*, 1st ed. (Academic Press, 2000).
[60] P. Coleman, *Introduction to Many-body Physics* (Cambridge University Press, 2015).
[61] F. Matsukura, Y. Tokura, and H. Ohno, Nat. Nanotechnol. **10**, 209 (2015).
[62] J. Bouaziz *et al.*, New J. Phys. **19**, 023010 (2017).